Laser and Particle Beams

cambridge.org/lpb

Effects of waveguides on a free-electron laser with two electron beams

Soon-Kwon Nam and Yunseong Park

Department of Physics, Kangwon National University, Chunchon 24341, Korea

Research Article

Cite this article: Nam S-K, Park Y (2019). Effects of waveguides on a free-electron laser with two electron beams. *Laser and Particle Beams* **37**, 386–391. https://doi.org/10.1017/S0263034619000557

Received: 1 May 2019
Revised: 18 May 2019
Accepted: 19 July 2019
First published online: 20 November 2019

Key words:
Free-electron laser; TE and TM modes; two electron beams; waveguide

Author for correspondence:
Soon-Kwon Nam, Department of Physics, Kangwon National University, Chunchon 24341, Korea, E-mail: snam@kangwon.ac.kr

Abstract

The effects of the phase variation, the evolution of the electron beam, the evolution of the radiation intensity, and the higher-order modes due to waveguides on a free-electron laser (FEL) oscillator have been analyzed by using two electron beams of different energies based on the proposed FEL facility which is to be operated in the far-infrared and infrared regions. The three-dimensional (3D) effects on a FEL oscillator due to waveguides and higher-order modes were studied using an extended 3D FEL code with two electron beams that we have developed. The effects of the variation on the amplitude of radiation on the electron beam's emittance and energy spreads were also calculated in the case of waveguide for multi-particle and multi-pass numbers by using a new 3D code. The phase variation, the variation in the beam envelope, the evolution of the amplitude, and power were calculated for the fundamental mode. The results were compared with those of the higher-order modes of the wiggler for various TE and TM modes for determining the FEL's performance which is required for high-quality electron beams.

Introduction

A free-electron laser (FEL) will operate from microwave through ultraviolet spectra, and relies upon stimulated scattering due to the ponderomotive potential created from the beating of the wiggler and radiation fields (Freund and Antonsen, 1996). The FEL power depends on the electron beam stability, the optical diffraction, and three-dimensional (3D) effects. The collective instability (Bonifacio *et al.*, 1984) and stability (Nam and Kim, 2010) of the electron beam play important roles in the electron beam and radiation field systems.

Theoretical studies on several waveguide types for FEL operation have been carried out at millimeter and sub-millimeter wavelength regions (Yakover *et al.*, 1996). The total electromagnetic field circulating in a resonator is represented as a superposition of transverse modes of the cavity. Coupled-mode theory was employed to derive a generalized 3D steady-state oscillation criterion from which the oscillator supermode (Pinhasi and Gover, 1996) can be found analytically in the linear gain approximation.

A quasi-3D time-dependent particle simulation (Sharp *et al.*, 1990) was developed to model slippage effects and waveguide effects on a single pass microwave FEL. The Gaussian mode is decomposed into the waveguide with TE and TM modes of the vacuum modes of a rectangular waveguide (Freund and Chang, 1990) and the subsequent evolution of both the multimode radiation field in the waveguide and the trajectories of the ensemble of electrons in the beam are followed self-consistently.

McNeil *et al.* (2004) proposed a single-pass two-beam FEL model. The model uses two electron beams with different energies in one-dimensional limit and shows an improved output coherence of the injected seed field. The higher energy electron beam is chosen so that its fundamental resonance wavelength is a harmonic resonance wavelength of the lower-energy beam.

In this paper, the 3D effects on a FEL oscillator due to the waveguide and higher-order modes are described for the nonlinear formulation of the interaction based on a two- beam system. We developed a code using an extended 3D model with two electron beams. The code includes TE and TM modes for the waveguide, as well as the electron beam's emittance, energy spread, betatron oscillations, and higher-order modes. The evolution of radiation field's intensity for the fundamental and higher-order modes for various TE and TM modes for the waveguide was studied. The effects of TE and TM modes for the waveguide on a proposed FEL facility that will be operated in the far-infrared and infrared regions were studied by using the extended 3D simulation code that we have developed. This paper also presents both the normalized FEL amplitude for the optimization of the beam's emittance and energy spread due to the TE and TM modes for the waveguide in a two-beam oscillator system.

CAMBRIDGE UNIVERSITY PRESS

Theory and formulation

The vector potential in a rectangular waveguide bounded by $-a/2 < x < a/2$ and $-b/2 < y < b/2$ may be written in the form of the TE and TM modes (Freund and Chang, 1990):

$$\delta\mathbf{A}(x, y, z, t) = \sum_{l,n}{}' \delta A_{l,n}(z)\mathbf{e}_{ln}^{(1)}(x, y)\cos\left[\alpha_{l,n}(z, t)\right] \tag{1}$$

$$\delta\mathbf{A}(x,y,z,t)=\sum_{l,n}^{\infty}\delta A_{l,n}\left(\mathbf{e}_{ln}^{(2)}(x,y)\cos\left[\alpha_{l,n}(z,t)\right]+\frac{\kappa_{l,n}}{k_{l,n}}\hat{e}_z\sin\left[\frac{l\pi X}{a}\right]\times\cos\left[\frac{n\pi Y}{b}\right]\sin\left[\alpha_{l,n}(z,t)\right]\right) \tag{2}$$

The summation symbol $\sum'$ indicates that both l and n may not be zero and l and n indicate the transverse mode numbers.

$$\alpha_{l,n}(z, t) = \int_0^z dz' k_{l,n}(z') - \omega t \tag{3}$$

$$\mathbf{e}_{ln}^{(1)}(x, y) = \frac{n\pi}{\kappa_{l,n}b}\hat{e}_x\cos\left[\frac{l\pi X}{a}\right]\sin\left[\frac{n\pi Y}{b}\right] - \frac{l\pi}{\kappa_{l,n}a}\hat{e}_y\sin\left[\frac{l\pi X}{a}\right]\times\cos\left[\frac{n\pi Y}{b}\right] \tag{4}$$

$$\mathbf{e}_{ln}^{(2)}(x, y) = \frac{l\pi}{\kappa_{l,n}a}\hat{e}_x\cos\left[\frac{l\pi X}{a}\right]\sin\left[\frac{n\pi Y}{b}\right] + \frac{n\pi}{\kappa_{l,n}b}\hat{e}_y\sin\left[\frac{l\pi X}{a}\right]\times\cos\left[\frac{n\pi Y}{b}\right] \tag{5}$$

where $X = x + a/2$ and $Y = y + a/2$.

The cutoff wave number of the mode is given by

$$\kappa_{l,n} = \pi\left[\frac{l^2}{a^2} + \frac{n^2}{b^2}\right]^{1/2} \tag{6}$$

Maxwell's equation is given by

$$\left(\frac{\partial^2}{\partial x^2} + \frac{\partial^2}{\partial y^2} + \frac{\partial^2}{\partial z^2} - \frac{1}{c^2}\frac{\partial^2}{\partial t^2}\right)\delta\mathbf{A}(x, y, z, t) = -\mu_0(\mathbf{J}^s + \mathbf{J}^f) \tag{7}$$

$$\begin{aligned}\mathbf{J}^i &= -e\sum_{j=1}^{N_e}\mathbf{v}_j^i\delta(x - x_j^i)\delta(y - y_j^i)\frac{\delta(t - \tau_j^i)}{|vz_j^i|}\\ &= -e\sum_{j=1}^{N_e}\gamma_j^i\mathbf{v}_j^i\delta(x - x_j^i)\delta(y - y_j^i)\frac{\delta(t - \tau_j^i)}{\gamma_j^i|vz_j^i|}\\ &= -e\sum_{j=1}^{N_e}\mathbf{u}_j^i\delta(x - x_j^i)\delta(y - y_j^i)\frac{\delta(t - \tau_j^i)}{|uz_j^i|} \quad i = s, f\end{aligned} \tag{8}$$

The symbols s and f indicate the slow beam (lower energy beam) and the fast beam (higher energy beam) respectively.

Substituting Eq. (1) into Eq. (7), averaging over the period $2\pi/\omega$ after multiplying by $\sin[\alpha_{l,n}(z, t)]$ and $\cos[\alpha_{l,n}(z, t)]$, integrating in x and y after obtaining the dot product with $\mathbf{e}_{ln}^{(1)}(x, y)$, multiplying by $4a^3b^3e\kappa_{l,n}^2\omega$ and $4abe\kappa_{l,n}^2\omega$, the ordinary differential equations for $\delta a_{l,n}$ and $k_{l,n}$ of the TE modes will be obtained:

$$-m\left(b^2l^2 + a^2n^2\right)\pi^3\left(\left(c^2\left(b^2l^2 + a^2n^2\right)\pi^2 - a^2b^2\omega^2 + a^2b^2c^2k_{l,n}^2\right) - a^2b^2c^2\frac{d^2}{dz^2}\right)\delta a_{l,n} = 4a^3b^3e\kappa_{l,n}^2\omega\left(s_{l,n}^{s,(1)} + s_{l,n}^{f,(1)}\right) \tag{9}$$

$$-c^2m\left(b^2l^2 + a^2n^2\right)\pi^3\left(\delta a_{l,n}\frac{d}{dz}(k_{l,n}) + 2k_{l,n}\frac{d}{dz}(\delta a_{l,n})\right) = 4abe\kappa_{l,n}^2\omega\left(s_{l,n,h}^{s,(2)} + s_{l,n,h}^{f,(2)}\right) \tag{10}$$

where $\delta a_{l,n} = e\delta A_{l,n}/mc^2$.

Substituting Eq. (2) into Eq. (7), averaging over the period $2\pi/\omega$ after obtaining the dot product with

$$\left(\mathbf{e}_{ln}^{(2)}(x, y)\cos\left[\alpha_{l,n}(z, t)\right] + \frac{\kappa_{l,n}}{k_{l,n}}\hat{e}_z\sin\left[\frac{l\pi X}{a}\right]\times\cos\left[\frac{n\pi Y}{b}\right]\sin\left[\alpha_{l,n}(z, t)\right]\right)$$

and

$$\left(\mathbf{e}_{ln}^{(2)}(x, y)\sin\left[\alpha_{l,n}(z, t)\right] + \frac{\kappa_{l,n}}{k_{l,n}}\hat{e}_z\sin\left[\frac{l\pi X}{a}\right]\times\cos\left[\frac{n\pi Y}{b}\right]\cos\left[\alpha_{l,n}(z, t)\right]\right),$$

integrating in x and y, assuming that $(d^2/dz^2)(k_{l,n})$ can be neglected, and multiplying by $4a^3b^3e\kappa_{l,n}^2\omega k_{l,n}^4$ and $4abe\kappa_{l,n}^2\omega k_{l,n}^2$, the ordinary differential equations for $\delta a_{l,n}$ and $k_{l,n}$ of the TM modes will be obtained.

The ordinary differential equations for $\delta a_{l,n}$ and $k_{l,n}$ of the TM modes will be obtained by

$$\begin{aligned}&m\pi(-a^2b^2c^2(b^2l^2+a^2n^2)\pi^2k_{l,n}^6\delta a_{l,n}\\ &+2a^4b^4c^2\kappa_{l,n}^4\left(\delta a_{l,n}\left(\frac{d}{dz}(k_{l,n})\right)^2 - k_{l,n}\frac{d}{dz}(k_{l,n})\frac{d}{dz}(\delta a_{l,n})\right)\\ &+a^2b^2\kappa_{l,n}^4k_{l,n}^2\left(-\left(c^2\left(b^2l^2+a^2n^2\right)\pi^2 - a^2b^2\omega^2\right)\delta a_{l,n}\right.\\ &\left.+a^2b^2c^2\frac{d^2}{dz^2}(\delta a_{l,n})\right)+k_{l,n}^4\left(-\left(c^2\left(\left(b^2l^2+a^2n^2\right)^2\pi^4+a^4b^4\kappa_{l,n}^4\right)\right.\right.\\ &\left.\left.-a^2b^2\left(b^2l^2+a^2n^2\right)\pi^2\omega^2\right)\delta a_{l,n}+a^2b^2c^2\left(b^2l^2+a^2n^2\right)\pi^2\frac{d^2}{dz^2}(\delta a_{l,n})\right)\\ &=4a^3b^3e\kappa_{l,n}\omega k_{l,n}^4\left(s_{l,n}^{s,(1)}+s_{l,n}^{f,(1)}\right)\end{aligned} \tag{11}$$

$$\begin{aligned}&-c^2m\pi\left(\left(a^2b^2\kappa_{l,n}^4+\left(b^2l^2+a^2n^2\right)\pi^2k_{l,n}^2\right)\delta a_{l,n}\frac{d}{dz}(k_{l,n})\right.\\ &\left.+2k_{l,n}\left(-a^2b^2\kappa_{l,n}^4+\left(b^2l^2+a^2n^2\right)\pi^2k_{l,n}^2\right)\frac{d}{dz}(r\delta a_{l,n})\right)\\ &=4abe\kappa_{l,n}\omega k_{l,n}^2\left(s_{l,n}^{s,(2)}+s_{l,n}^{f,(2)}\right)\end{aligned} \tag{12}$$

https://doi.org/10.1017/S0263034619000557 Published online by Cambridge University Press

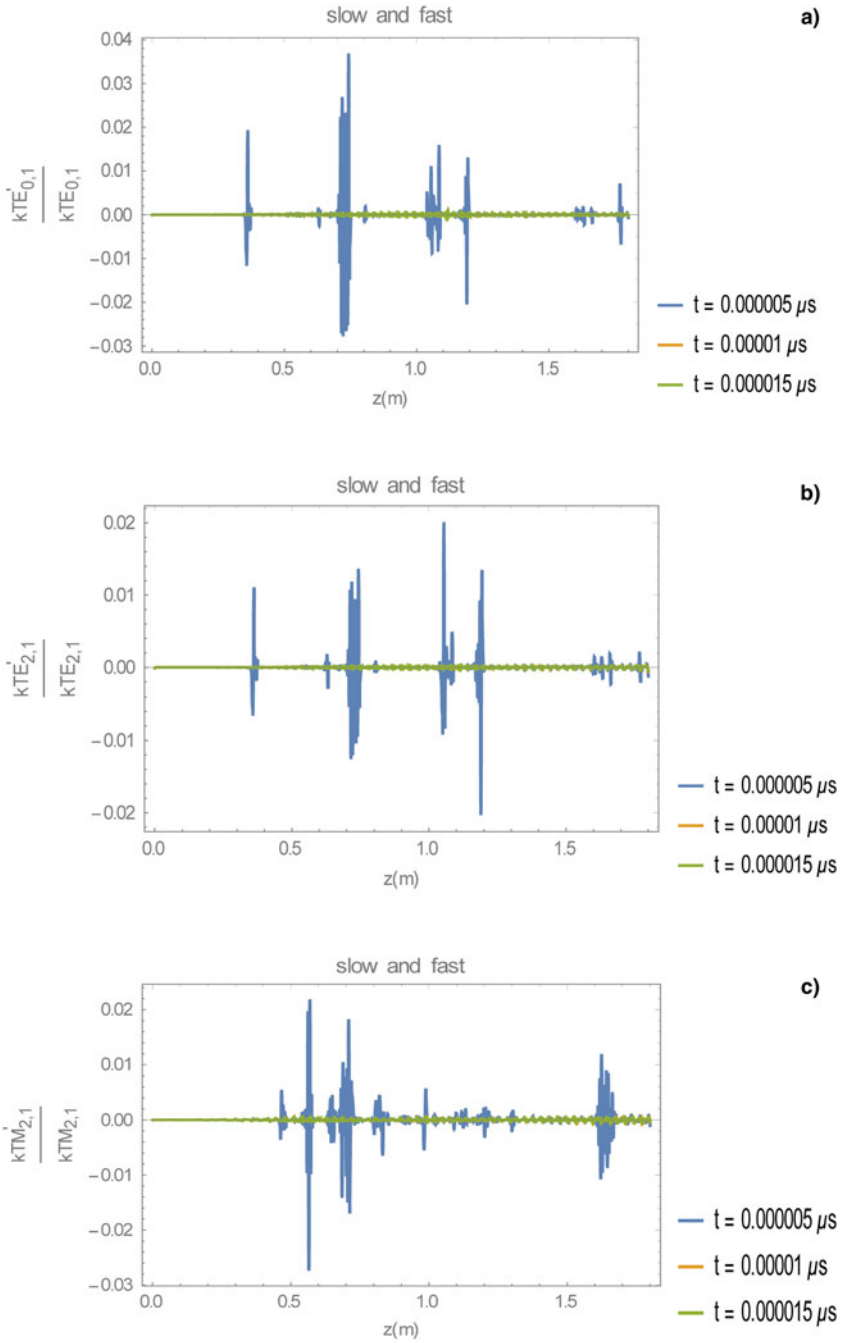

Fig. 1. The ratio of the derivative of the wave number and the wave number for (a) TE_{01}, (b) TE_{21}, and (c) TM_{21} modes.

The source terms are given by

$$s_{l,n}^{i,(1)} = -e\mu_0 \sum_{j=1}^{N_e} \frac{\mathbf{u}_j^i}{|uz_j^i|} \cdot \mathbf{e}_{ln}^{(1)}\left(x_j^i, y_j^i\right) \cos\left[\alpha_{l,n}\left(z, \tau_j^i\right)\right] \quad i = s, f \tag{13}$$

$$s_{l,n}^{i,(2)} = -e\mu_0 \sum_{j=1}^{N_e} \frac{\mathbf{u}_j^i}{|uz_j^i|} \cdot \mathbf{e}_{ln}^{(1)}\left(x_j^i, y_j^i\right) \sin\left[\alpha_{l,n}\left(z, \tau_j^i\right)\right] \quad i = s, f \tag{14}$$

In time-dependent simulation, the radiation in the ith slice is replaced by

$$\delta A_i \rightarrow \delta A_i - (\delta z/\lambda_w)(\lambda/c\Delta t) \times [\delta A_i - \delta A_{i-1}] \tag{15}$$

The numerical analysis and simulations

The parameters of our simulation were an undulator period 2 cm; a number of periods of 100; beam currents (I_b) of 75 and 25 A for $n = 3$, respectively; a radius of curvature 450–520 cm; and a resonator length of 8.0 m. The simulation used our extended 3D simulation code, which describes the effects of two-electron beams

https://doi.org/10.1017/S0263034619000557 Published online by Cambridge University Press

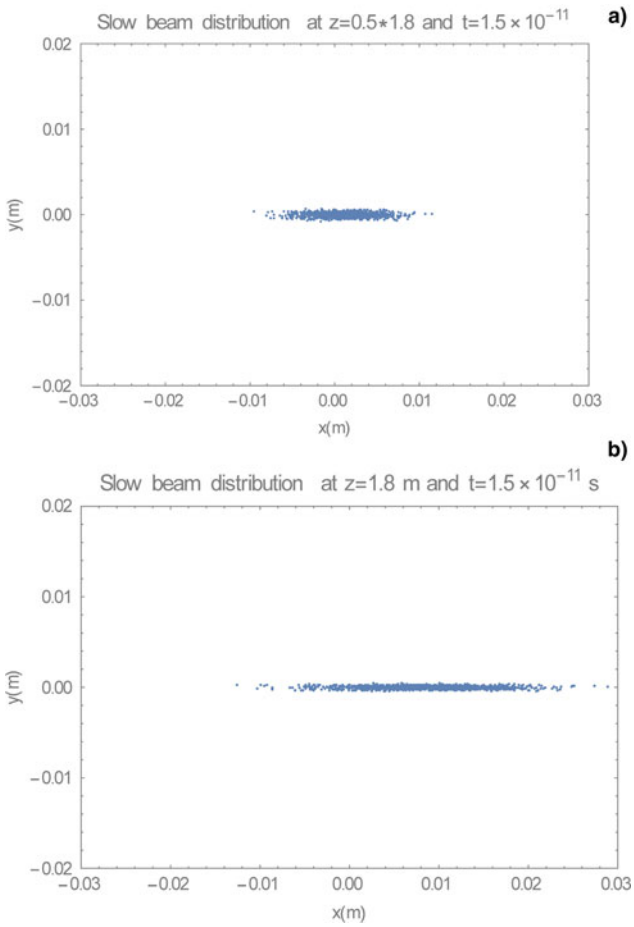

Fig. 2. The slow electron beam cross-sections at the center (a) and at the end (b) of wiggler for the total modes with TE_{01}, TE_{21}, and TM_{21} modes for the two-beam system with an emittance of $\varepsilon_n = 10$ mm · mradand an energy spread of 0.1%.

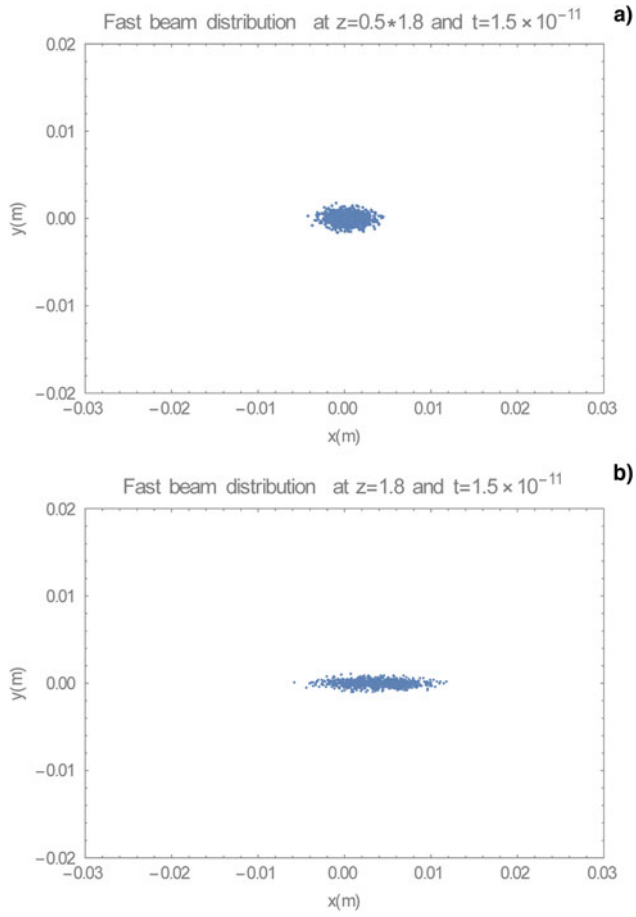

Fig. 3. The fast electron beam cross-sections at the center (a) and at the end (b) of wiggler for the total modes with TE_{01}, TE_{21}, and TM_{21} modes for the two-beam system with an emittance of $\varepsilon_n = 10$ mm · mradand an energy spread of 0.1%.

with different energies, i.e., 10.4 MeV (higher-energy beam) and 6 MeV (lower-energy beam). The seed field at the lower electron beam energy is modeled by defining its initial scaled intensity at the beginning of the FEL interaction to be two orders of magnitude greater than that of the harmonic. Multi-particle and multi-pass simulations were performed for a particle number of 200 and a pass number of 300. In the simulations, the minimum waist position of the radiation is at the center of the cavity. The radiation spot size (w_0) at minimum waist, higher order modes, and the number of macro-particles ($j = 200$) were used in the simulations.

The differential equations governing each mode are integrated simultaneously with the 3D Lorentz force equations for an ensemble of electrons subject to the wiggler, electromagnetic, and static self-fields of the beam.

These equations describe the gain and refractive guiding of the signal. An arbitrary optical signal may be represented by an ensemble of the vacuum waveguide modes which satisfies the boundary conditions of the electromagnetic field imposed by the waveguide wall. The FEL interaction will cause each mode in the ensemble to either grow or decay at different rates. The relative amplitudes and the evolution of wave number for each TE and TM modes will vary over the course of the interaction and will alter the radiation profile to describe the optical guiding of the signal. The refractive guiding is presented by the waveguide

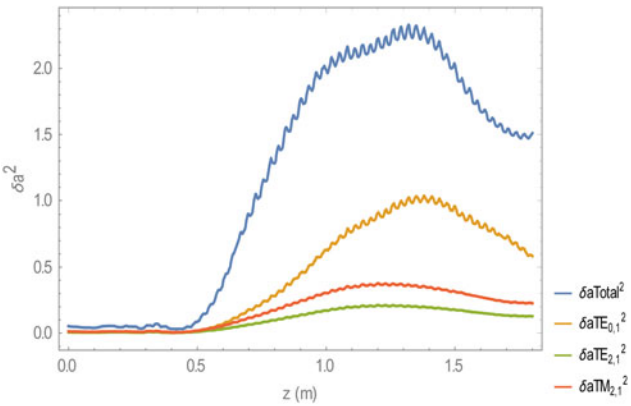

Fig. 4. Evolutions of the radiation field intensity for the total modes with TE_{01}, TE_{21}, and TM_{21} modes in the two-beam system with an emittance of $\varepsilon_n = 10$ mm · mrad and an energy spread of 0.1%.

mode representation because variations of the wave number result in the corresponding variations under the wave-particle resonance conditions that alter the individual growth and damping rates of various modes.

The phase variation is related to the refractive guiding of the signal which is included in the general 3D formulation. The

https://doi.org/10.1017/S0263034619000557 Published online by Cambridge University Press

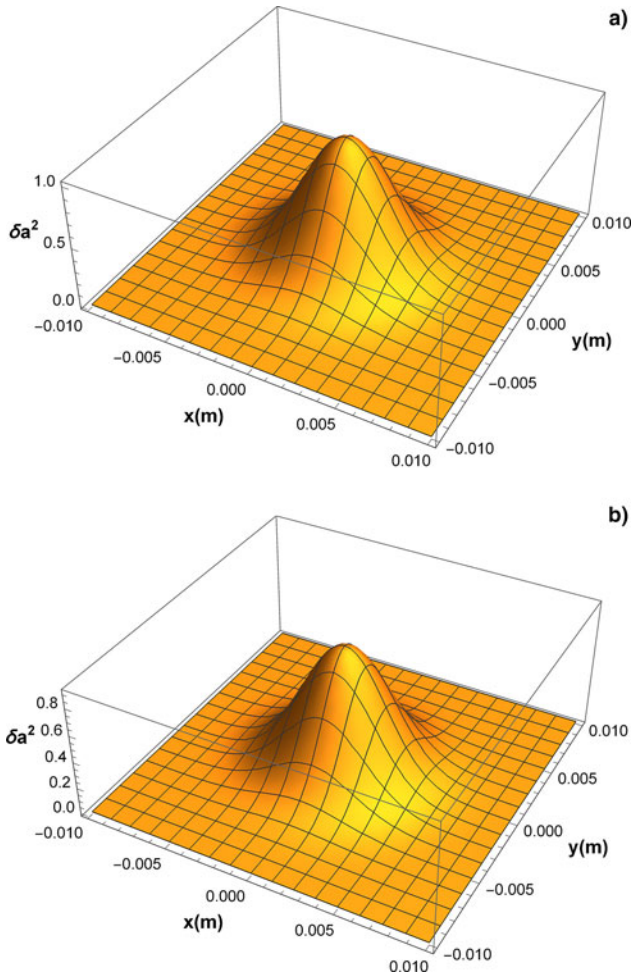

Fig. 5. Evolutions of the radiation field intensity for the total modes with TE_{01}, TE_{21}, and TM_{21} modes in the two-beam system (a) and the single beam system (b) with an emittance of $\varepsilon_n = 10$ mm · mradand an energy spread of 0.1%.

ratio of the derivative of the wave number and the wave number for each TE_{ln} and TM_{ln} modes are shown in Figure 1 using the 3D time-dependent simulations which we have developed.

The states of the electron beam are illustrated in Figure 2. The evolution of the electron beam in this system describes the effects of the wiggler-induced oscillation on the transverse and axial velocities, and the wiggler gradients on the variation in the beam envelope due to the betatron oscillations. We plot the loading of the slow electron beams at the center of wiggler and at the end of wiggler as shown in Figure 2.

The fast electron beam cross-sections are shown in Figure 3 at the center of wiggler and at the end of wiggler. The cross-sections of the fast electron beam are much shorter than those of the slow beam. However, the cross-section of beam at the end of wiggler after saturation is longer than that of the electron beam at the center of the wiggler.

The evolution of the radiation intensity with axial distance for the total, TE_{01}, TE_{21}, and TM_{21} modes is shown in Figure 4 for a two-beam system.

As shown in the figure, the radiation intensity saturates at $z =$ 1.3 m with the relative field intensity level of approximately 2.5. This represents a much lower growth rate and efficiency than found for either of the TE and TM mode, despite the fact that the cutoff frequency and dispersion curves are degenerate for TE_{21} and TM_{21} modes. The difference between the two modes lies in the transverse mode structure.

Evolution of the radiation field intensity in the x and y planes for the total modes including TE_{01},TE_{21}, and TM_{21} modes with an emittance of $\varepsilon_n = 10$ mm · mradand energy spread of 0.1% in the two-beam oscillator system is shown in Figure 5(a) and the result is compared with that of a single beam system as shown in Figure 5(b).

Evolution of the radiation field intensity in the single beam system has lower radiation amplitudes relative to that in the higher energy beam with a two-beam oscillator. For an emittance of $\varepsilon_n = 10$ mm · mradand energy spread of 0.1%, the saturation intensity $|A|^2$ of the single beam with TE_{01}, TE_{21}, and TM_{21} modes at 200 particles and 300 passes decreased by approximately 11% relative to that for the two beams.

Evolutions of the total power with passes of 300 and 200 particles are shown in Figure 6 for the case of two electron beams. All resonant modes which are restricted to the TE_{01}, TE_{21}, and TM_{21} modes are simultaneously included in the simulation. As observed in the figure, the total power saturates at a level of approximately 2 GW after 300 passes. It is also evident that although the TE_{01} mode was overwhelmingly dominant upon the injection of the signal, it comprises only approximately 68% of the power at saturation. The remaining powers are composed of theTE_{21} and TM_{21} modes which are less than approximately 11%.

This is due to the fact that the growth rates of the TE_{21} and TM_{21} modes are higher than that of the TE_{01} mode at this frequency.

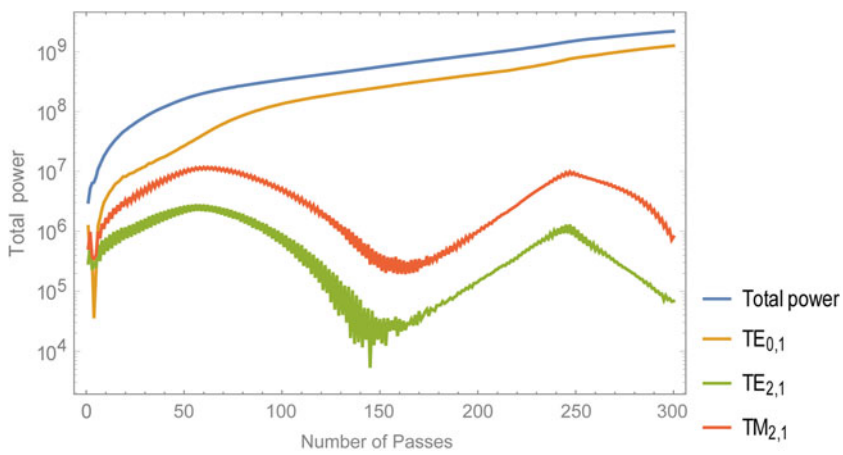

Fig. 6. Evolutions of the total power for the total modes, TE_{01}, TE_{21}, and TM_{21} modes for the two-beam system with an emittance of $\varepsilon_n = 10$ mm · mradand an energy spread of 0.1%.

https://doi.org/10.1017/S0263034619000557 Published online by Cambridge University Press

Conclusions

The 3D effects on a FEL oscillator with the waveguide were studied for the phase variation, the evolution of the electron beam, the evolution of the radiation intensity, and the higher-order modes by using an extended 3D FEL code with two electron beams that we have developed.

A set of coupled nonlinear differential equations was derived for the evolution of each mode which is integrated in conjunction with the 3D Lorentz force equations for an ensemble of electrons.

The ratios of the derivative of the wave number and the wave number for each TE_{ln} and TM_{ln} mode were calculated by the 3D time-dependent simulations which we have developed.

The states of the electron beam were also studied for the loading of the slow electron beams at the center of wiggler and at the end of wiggler. The results were compared with those of the fast electron beams to analysis the wiggler-induced oscillation in the transverse and axial velocities.

The evolution of the radiation intensity with axial distance for the total modes, TE_{01}, TE_{21}, and TM_{21} modes was calculated for two-beam system. The radiation intensity saturates at $z = 1.3$ m with the relative field intensity level of approximately 2.5. This represents a much lower growth rate and efficiency than found for either of the TE and TM mode, despite the fact that the cutoff frequency and dispersion curves are degenerate for the TE_{21} and TM_{21} modes.

For an optimized emittance of $\varepsilon_n = 10$ mm · mradand energy spread of 0.1%, the saturation intensity of the single beam with TE_{01}, TE_{21}, and TM_{21} modes at 200 particles and 300 passes decreased by approximately 11% relative to that for the coupled two-beam oscillator system.

The radiation field's intensity for the higher-order modes was highly sensitive compared with the fundamental mode of waveguide; however, it was less sensitive to the emittance and the energy spread for the coupled two-beam oscillator system.

Acknowledgements. This research was supported by the Basic Science Research Program through the National Research Foundation of Korea (NRF) funded by the Ministry of Science (NRF-2017R1A2B4002015).

References

Bonifacio R, Pelligrini C and Narducci LM (1984) Collective instabilities and high-gain regime in a free electron laser. *Optics Communications* **50**, 373.

Freund HP and Antonsen TM (1996) *Principles of Free-Electron Lasers*. London: Chapman & Hall.

Freund HP and Chang CL (1990) Effects of the lower beat wave on optical guiding in planar wiggler free electron lasers. *Physical Review A* **42**, 6737.

McNeil BWJ, Robb GRM and Poole MW (2004) Two-beam free electron lase. *Physical Review A* **70**, 035501.

Nam S and Kim K (2010) Stability of an electron beam in a two-frequency wiggler with a self-generated field. *Journal of Plasma Physics* **77**, 257.

Pinhasi Y and Gover A (1996) Transverse mode coupling and supermode establishment in a free-electron laser oscillator. *Nuclear Instruments and Methods in Physics Research A* **375**, 233.

Sharp WM and Yu SS, Pierini P and Cerchioni G (1990) Waveguide effects in superradiant free-electron lasers. *Nuclear Instruments and Methods in Physics Research A* **296**, 535–544.

Yakover IM, Pinhasi Y and Gover A. (1996) Study of waveguide resonators for FEL operating at submillimeter wavelengths. *Nuclear Instruments and Methods in Physics Research A* **375**, 260–263.

https://doi.org/10.1017/S0263034619000557 Published online by Cambridge University Press